GEOPHYSICS, VOL. 76, NO. 2 (MARCH-APRIL 2011); P. F89–F99, 10 FIGS.
10.1190/1.3536641

Three methods for mitigating airwaves in shallow water marine controlled-source electromagnetic data

Jiuping Chen[1] and David L. Alumbaugh[1]

ABSTRACT

In the past several years, marine controlled-source electromagnetic (MCSEM) techniques have been applied successfully in deep water (depth $>$ 1 km) for oil and gas exploration. The application of this technology in shallow water is challenged, however, because of "airwaves" that mask the signal from the target reservoir at depth. Based upon the understanding that an airwave is a lateral wave, which can be analytically expressed in a dual-half-space resistivity model, we propose three airwave-mitigation approaches to reduce the effects of these airwaves on MCSEM data. In the EM "x-bucking" approach, the effect of the airwaves can be "bucked" out from two measurements by using the analytic expression of the airwave. The frequency derivative (dE/dFreq) approach takes advantages of the unique characteristics of the airwaves in frequency domain, enhancing the reservoir signals while suppressing the airwave. The magnetotelluric (MT) stripping method uses the plane-wave feature of the airwaves and subtraction of the lateral wave electric component, which is obtained from measured marine MT impedance and controlled-source electromagnetics (CSEM) data, to generate a new data set in which the effects of the airwaves are removed substantially. By comparing the detectability, which is defined as the ratio of inline E_x fields between a reservoir model and a corresponding baseline model, for a reservoir target in deep water versus shallow water with a moderate 2D bathymetry, we show that the effects of the airwaves in shallow water can be reduced in the data, leading to greater reservoir detectability. In addition, these approaches have been applied successfully to a real shallow water MCSEM data set in which the detectability to the deeper resistive basement is enhanced.

INTRODUCTION

Marine controlled-source electromagnetics (MCSEM) have been applied to de-risk deepwater oil and gas exploration. This method uses a high-powered horizontal electric dipole (HED) to transmit a low-frequency (0.01–10 Hz) EM signal through the seawater column and seafloor. The transmitting source (Tx) typically is towed just above an array of multicomponent EM receivers (Rx) that are deployed on the seafloor to record the EM responses. By analyzing these EM responses, the bulk electrical resistivity of seafloor sediments can be estimated as a function of lateral position and, more importantly, depth. Because oil and gas are relatively resistive compared to fluid-filled conductive sediments, the resulting analysis can be used to infer whether a given region of the subsurface contains hydrocarbon (Young and Cox, 1981; Chave and Cox, 1982; Eidesmo et al., 2002; Srnka et al., 2006).

The depth of the seawater column has a strong influence on measured EM signals. Because of this, early applications of MCSEM for hydrocarbon exploration concentrated on targets in deepwater scenarios, where the water depth generally is greater than 1 km (Andréis and MacGregor, 2008). Conventional transmitters are towed deep to maximize EM coupling between sources, receivers and reservoir targets, as well as to mitigate so-called "airwave" effects (Constable, 2003; Lu et al., 2005; Løseth et al., 2008).

The airwave effect is notorious in shallow water (depth $<$ 300 m), where the useful signals from the reservoir targets might be masked totally by the airwave, which generally contains little information about the subsurface. This is illustrated in Figure 1,

Manuscript received by the Editor 14 May 2010; revised manuscript received 7 September 2010; published online 25 February 2011.
[1]Schlumberger-EMI Technology Center, Berkeley, California, U.S.A. E-mail: jchen16@slb.com; dalumbaugh@slb.com.
© 2011 Society of Exploration Geophysicists. All rights reserved.

Downloaded 11 Jun 2012 to 146.23.4.26. Redistribution subject to SEG license or copyright; see Terms of Use at http://segdl.org/

where the magnitudes of the inline electric field (E_x) versus Rx-Tx offset (MVO) are plotted in Figure 1c and d for a deepwater and shallow water scenario.

Each scenario consists of two models: One is the "target" model where the hydrocarbon reservoir is present, and the other the "baseline" model where the reservoir is absent. Figure 1a and b show the target models in the corresponding water scenarios.

Five frequencies, from 0.18 to 0.56 Hz, were used in this analysis. The conventional normalized responses between a target and baseline models are displayed in Figure 1e and f as well. In these two scenarios, the hydrocarbon reservoir example is identical; the difference lies only in the water depth: 3000 m for the deepwater and 100 m for the shallow water case. In deep water, fields tend to attenuate more rapidly with increasing offset. Also, the separation between the target and baseline responses is visually obvious.

In shallow water, on the other hand, the attenuation of the fields with offset is much slower, and it is difficult to distinguish between the target and baseline responses. In Figure 1e and f, the magnitude of the normalized responses in the deep water goes as high as 4.0 at all five frequencies, suggesting that the reservoir clearly is detectable in this case. By contrast, the shallow water responses are nearly united, indicating that it would be more difficult to detect the reservoir in this scenario.

Because the airwave masks the deeper reservoir signal, much effort has been devoted to removing it from observed measurements. The usefulness of this approach for simple data visualization and presentation generally is accepted in the EM community, although its added value as a whole for interpretation is a topic of extensive debate.

Several techniques have been published for dealing with frequency-domain (FD) EM data. These include upward and downward separation of the measured fields (Amundsen, 2003), measurement of vertical electric fields (Constable, 2003), combining spatial derivatives of the measured electric and magnetic fields (MacGregor et al., 2005), subtraction of a background model response from a total field (Lu et al., 2005), direct computation of the airwaves (Nordskag and Amundsen, 2007; Weidelt, 2007), using crossed-dipole sources (Løseth and Amundsen, 2007), and using reciprocity/decomposition of EM fields (van den Berg et al., 2008). In the time domain (TD), the airwaves are considered to be separable in the early time data (Ziolkowski and Wright, 2007), although their effects still might prevail and interfere with other components in the midtime range (Weiss, 2007).

Based upon the understanding of the airwave as a "lateral wave" (Clough, 1976; Bannister, 1984; King et al., 1992), we propose three new airwave-mitigation methods. These are (1) EM bucking or x-bucking, (2) frequency derivative (dE/dFreq), and (3) magnetotelluric (MT) impedance stripping approaches. We introduce each method and then analyze the ability of these approaches to mitigate the airwave by applying them to

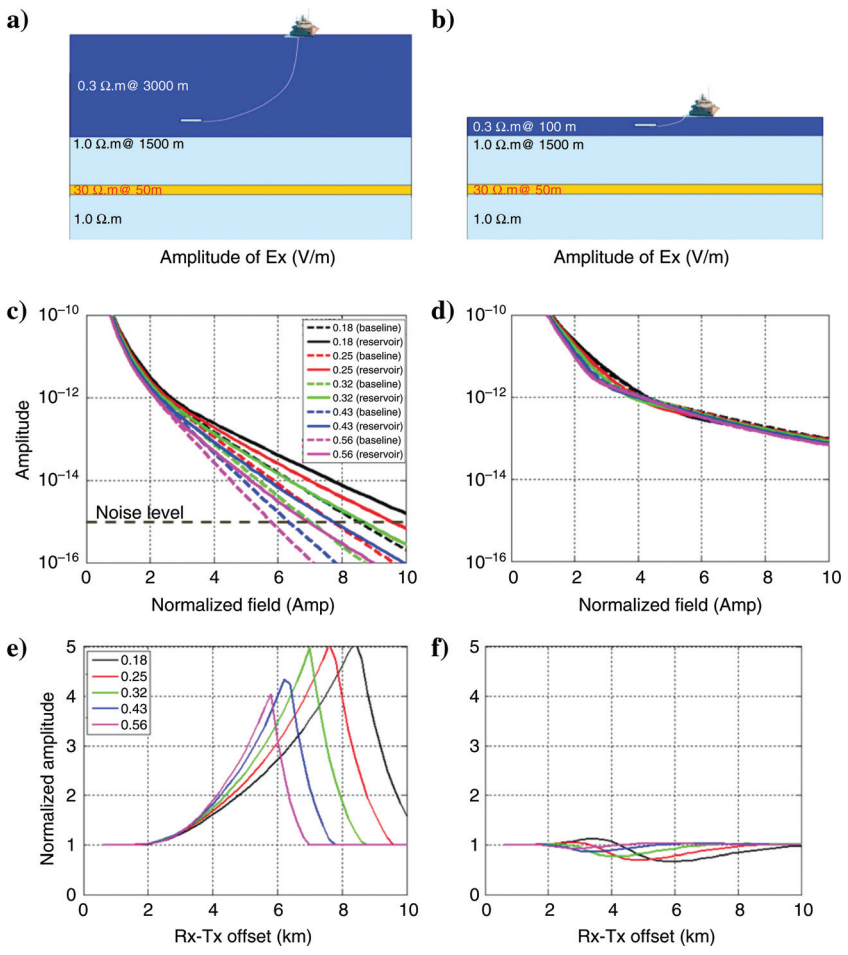

Figure 1. An example showing the differences in the MCSEM fields for a deepwater and a shallow water scenario. Figure 1a is the deepwater model, in which the water depth is 3000 m, and 1b is the corresponding shallow water where the water depth is 100 m. Figure 1c and d show the magnitudes of the inline E_x versus Rx-Tx offset (MVO) for the target and baseline models in each water scenario. Figure 1e and f show the normalized amplitudes for deep water and shallow water. Five frequencies range from 0.18 to 0.56 Hz. Note that for computing the normalized responses, a noise level of 1.0×10^{-15} V/m was used as a cutoff value.

Downloaded 11 Jun 2012 to 146.23.4.26. Redistribution subject to SEG license or copyright; see Terms of Use at http://segdl.org/

synthetic shallow water FD MCSEM data. These FD data were generated from synthetic 2D models in deep (water depth 3 km) and shallow (100 m) water, coupled with a flat and bathymetric mudline. Comparing deepwater, shallow water, and airwave-mitigated shallow water responses, with and without realistic bathymetry, provides the detectability analysis.

We then validate these approaches on a real MCSEM data set acquired in shallow water. By using the time-domain EM data, which are believed to be less affected by the airwave, we come up with a representative 1D resistivity model which has a fairly high resistive basement. Similar to the detectability analysis done in the synthetic 2D model study, we show that by mitigating the airwave effect the detectability to the deep resistive basement can be enhanced compared with the detectability in the raw measurements.

We conclude the paper with a discussion.

'LATERAL-WAVE' THEORY

Bannister (1984) derives explicit approximate expressions for the EM radial electric field produced by a horizontal electric dipole (HED) source in a dual-half-space model in which the electromagnetic fields can be broken into three components (Figure 2): a direct component (D), a modified image component (I), and "lateral wave" (L). These three components can be distinguished from their exponential decay terms, which are manifested analytically:

$$\begin{aligned} E_\rho(\rho,z,\phi) &= D+I+L=\frac{p\cos\phi}{2\pi\sigma\rho^3} \\ &\times\left\{\left[(1+k\rho)-\left(3+3k\rho+k^2\rho^2\right)\frac{(z-h)^2}{2\rho^2}\right]e^{-kR_0}\right. \\ &-\left[\left(3+3k\rho+k^2\rho^2\right)\frac{(z+h)^2}{2\rho^2}\right]e^{-kR_1} \\ &\left.+\left[\left(1+k_0\rho+k_0^2\rho^2F\right)\right]e^{-k_0\rho}e^{-k(z+h)}\right\}. \end{aligned} \tag{1}$$

For the convenience of using these components in the following derivations, we explicitly list each component as

$$D=\frac{p\cos\phi}{2\pi\sigma\rho^3}\left\{\left[(1+k\rho)-\left(3+3k\rho+k^2\rho^2\right)\frac{(z-h)^2}{2\rho^2}\right]e^{-kR_0}\right\}, \tag{2}$$

$$I=\frac{p\cos\phi}{2\pi\sigma\rho^3}\left\{-\left[\left(3+3k\rho+k^2\rho^2\right)\frac{(z+h)^2}{2\rho^2}\right]e^{-kR_1}\right\}, \tag{3}$$

and

$$L=\frac{p\cos\phi}{2\pi\sigma\rho^3}\left\{\left[\left(1+k_0\rho+k_0^2\rho^2F\right)\right]e^{-k_0\rho}e^{-k(z+h)}\right\}. \tag{4}$$

In these equations, p is the dipole moment for the HED, ρ is the radial distance between the receiver (Rx) and the HED, z is the vertical depth of the receiver below the water top surface, ϕ is the azimuthal angle between the HED and the receiver position (for inline mode, $\phi=0$), and h is the vertical depth of the HED source. The physical property σ is the electrical conductivity of the water, k is the wavenumber in the water, which is expressed as

$$k=\sqrt{i\omega\mu_0\sigma}, \tag{5}$$

in which ω is the angular frequency, which relates to the frequency f of the operation as $\omega=2\pi f$, $i=\sqrt{-1}$, and μ_0 is the magnetic permeability in the free space ($4\pi\times10^{-7}$ H). Similarly k_0 is the wavenumber in free space, which has an expression

$$k_0=i\omega\sqrt{\mu_0\varepsilon_0}\approx i2.1f\times10^{-8}, \tag{6}$$

and ε_0 is the dielectric permittivity in the free space (8.854×10^{-12} W/m).

As shown in Figure 2, R_0 is the distance between the receiver and the HED, which is computed as

$$R_0=\sqrt{\rho^2+(z-h)^2}, \tag{7}$$

and R_1 is the distance between the receiver and the mirror image source, which is given as

$$R_1=\sqrt{\rho^2+(z+h)^2}. \tag{8}$$

The symbol F is the Sommerfeld surface-wave attenuation function (Wait, 1961), which can be approximated as $F\cong1.0$ for small numerical distances. This is true for the case in which the frequency is low (<100 Hz), and the offset between the transmitter and receiver generally is less than 100 km. Another quantity used here is the skin depth (δ) in the water, which can be calculated as

$$\delta=\sqrt{\frac{2}{\omega\mu_0\sigma}}\approx503\sqrt{\frac{1}{f\sigma}}. \tag{9}$$

Notice that the assumptions made in equation 1 are

$$\left\|n^2\right\|=\left\|\frac{k^2}{k_0^2}\right\|\geq10, \tag{10}$$

where n is the index of refraction, and

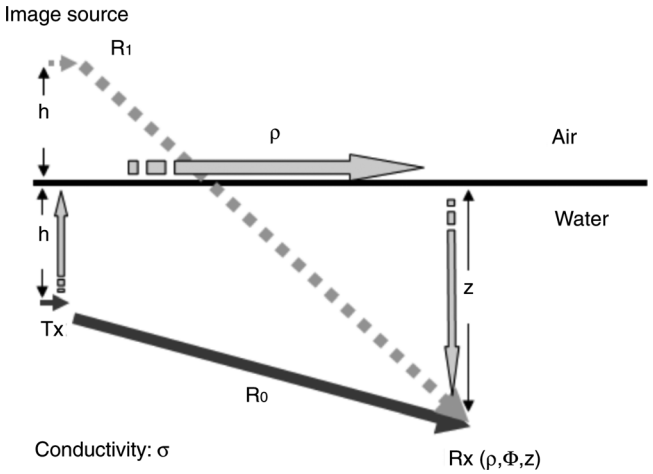

Figure 2. A schematic of EM fields due to a horizontal electric dipole (HED) source in a dual half-space model. The travel paths of the three components: direct field (D), modified image field (I), and "lateral wave" (L) are denoted by the solid, dashed, and upward-interface-downward arrows, respectively.

Downloaded 11 Jun 2012 to 146.23.4.26. Redistribution subject to SEG license or copyright; see Terms of Use at http://segdl.org/

$$\rho \geq 3(z+h). \tag{11}$$

It is easy to estimate

$$\left\|n^2\right\| = \frac{\sigma}{\omega\varepsilon_0} \approx 2.4 \times 10^{11}, \tag{12}$$

when $\sigma = 3.3$ S/m, and $f = 0.25$ Hz. Therefore there is no need to worry about the first assumption.

The direct field, which contains e^{-kR_0}, is shown in equation 2. The reflected or modified image field is provided in equation 3, and is expressed with the exponential term e^{-kR_1}. As shown in Figure 2, R_1 is the distance between the image source location (in the air) and the Rx. The last component shown in equation 4 is the most interesting because it has an upward path (e^{-kh}), a path traveling along the interface of the air and water $\left(e^{-k_0\rho}\right)$, and a downward path ($e^{-kz}$). This is the so-called lateral wave (Clough, 1976; Bannister, 1984; King et al., 1992).

For the upward and downward segments, we can see that the field is traveling in water with a wavenumber k in the exponential terms e^{-kh} and e^{-kz}, which is similar to a vertically traveling plane wave assumed in the MT method. But the segment traveling above the interface propagates with a wavenumber equivalent to that of air.

Because $|k_0|$ in the air is much smaller than $|k|$ in water, the geometric attenuation along the surface is negligible, and thus the only electromagnetic attenuation for the lateral wave occurs in the upward and downward segments, which are related directly to the depths of the Tx and Rx.

We believe that this lateral wave, which describes the physics of the so-called airwave in the dual-half-space model, can be extended empirically to more complicated cases as the dominant conductivity contrast in this marine controlled-source electromagnetics (CSEM) scenario is provided by the air-seawater interface. For a more realistic 1D model, Nordskag and Amundsen (2007) describe asymptotic expressions for the interactions between the airwave and the coupling (reflections and reverberations) to a layered subsurface. It is shown that the airwave with surface coupling still has the characteristics of a lateral wave. In addition, for general 2D and 3D models where the airwave is coupled to the subseafloor and formations in a more complicated way, it would be difficult to separate the airwave part explicitly. However, we believe that expression 1 provides at least a first-order approximation for the airwaves in these cases, and provides valuable information on its spatial decay, frequency and plane-wave characteristics. We explore this in the following sections.

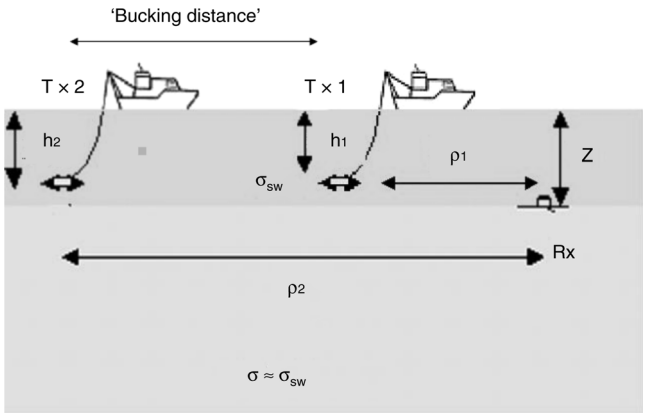

Figure 3. A schematic of applying the "bucking" or "x-bucking" method to removing the effect of airwave in a MCSEM survey. Assume that the water conductivity σ_{sw} is close to the conductivity σ of the seabed formation. Then two separated transmitters can be used to "buck" out the airwave recorded in the receiver. The horizontal distance between the two transmitters is called the "bucking distance."

In deep water, the sum of h and z essentially is two times the water depth. Therefore the interactions among the direct, image, and airwave fields are manifested in the relationship of ρ and $h+z$. In near offsets, i.e., $\rho \ll h+z$, the direct and image fields are dominant in measurements, and the airwave part can be ignored. At large offsets, for example, when $\rho \gg h+z$, the direct and image fields are attenuated heavily, and the remaining field is the airwave. This explains why the airwave becomes dominant at far offsets. In between these two extremes, all three components are present with none dominant.

In contrast, for shallow water surveys, Tx and Rx are close to the air/water interface; h and z must be much smaller than the horizontal distance ρ. Therefore, when the horizontal distance is large, we expect to see that the airwave dominates the total field, making it difficult to infer subsurface resistivity information from measurements. However, we can make use of certain characteristics of equation 1 to develop methods to mitigate theses effects.

THREE AIRWAVE-MITIGATION APPROACHES

Approach 1: EM 'bucking'

As shown in Figure 3, for a given towline where the receiver (Rx) depth z remains constant, we see from equation 4 that the airwave depends only on the horizontal distance between the source and receiver, ρ, the depth of the transmitter (Tx), h, and the wavenumber k in the water. Thus if we have fairly accurate estimates of σ, ρ and h, we can cancel, or "buck out," the airwave by combining multiple measurements.

Here we use two measurements, E_1 and E_2 at the same Rx but with two Tx positions, using the expression

$$E_{12}^{b} = E_1 \cdot e^{-k(h_2-h_1)}\left(\frac{\rho_1}{\rho_2}\right)^3 - E_2, \tag{13}$$

where ρ_1 and h_1 represent positions of the first Tx relative to the receiver, and ρ_2 and h_2 are the second Tx position. The usefulness of this approach relies on the reservoir response having a different geometrical fall-off versus source-receiver separation compared to the airwave, which generally is the case. The horizontal distance between two transmitters used for removing the effect of the airwave is referred to as bucking or x-bucking distance. Similarly, we can apply this idea to two measurements associated with two Rxs but with the same Tx position.

Here we use the analytic expression for the airwave in a dual-half-space model. As mentioned above, Nordskag and Amundsen (2007) proved that the airwave still behaves like a lateral wave in a realistic 1D model. The assumption and restrictions on the water and seabed conductivity, as well as the effect from the water column conductivity, might be lessened. Because the transmitter is towed in the water, the uncertainty on the depth of the transmitter, as well as the variation of the source angle,

Downloaded 11 Jun 2012 to 146.23.4.26. Redistribution subject to SEG license or copyright; see Terms of Use at http://segdl.org/

might have more severe implications on the removal of the airwave by bucking. All these complications will affect how this bucking approach works on MCSEM data, which is discussed in the synthetic and real data sections.

Approach 2: dE/dFreq

In equations 2 to 4, we have the explicit expressions for the direct-wave (D), modified image (I), and lateral wave (L) for the radial component of the electrical field generated from a HED. Now we want to take the derivatives of each part with respect to angular frequency. During the derivation, we make use of the following equations

$$\frac{\partial k}{\partial \omega} = \frac{i\mu\sigma}{2k} = \frac{1}{2\omega}\frac{1+i}{\delta}, \tag{14}$$

and

$$\frac{\partial k_0}{\partial \omega} = i\sqrt{\mu_0 \varepsilon_0} \approx i3.33 \times 10^{-9}. \tag{15}$$

Taking derivatives of equations 2, 3, and 4 leads to simplified expressions

$$\frac{\partial D}{\partial \omega} = \alpha_D \cdot D, \tag{16}$$

$$\frac{\partial I}{\partial \omega} = \alpha_I \cdot I, \tag{17}$$

and

$$\frac{\partial L}{\partial \omega} = \alpha_L \cdot L, \tag{18}$$

with coefficients

$$\alpha_D = -\frac{1+i}{2\omega}\cdot\frac{\rho}{\delta}\left[1 - \frac{1-(3+2k\rho)\frac{(z-h)^2}{2\rho^2}}{(1+k\rho)-(3+3k\rho+k^2\rho^2)\frac{(z-h)^2}{2\rho^2}}\right], \tag{19}$$

$$\alpha_I = -\frac{1+i}{2\omega}\cdot\frac{\rho}{\delta}\left[1 - \frac{3+2k\rho}{3+3k\rho+k^2\rho^2}\right], \tag{20}$$

and

$$\alpha_L = -\frac{1+i}{2\omega}\cdot\frac{z+h}{\delta}. \tag{21}$$

Thus

$$\frac{\partial E_\rho}{\partial \omega} = \alpha_D \cdot D + \alpha_I \cdot I + \alpha_L \cdot L. \tag{22}$$

This means that compared with the original radial E_ρ field, the attenuation or enhancement in the derivatives is controlled by three coefficients, which can be analyzed further as follows.

In shallow water scenarios, the depth between transmitter and receiver is much smaller than the Tx-Rx offset ρ in the offset range of interest, say, from 2 km to 20 km. This means that if

$$|k\rho| = \left|\sqrt{i\omega\mu_0\sigma}\rho\right| = \left|(1+i)\frac{\rho}{\delta}\right| = \frac{\sqrt{2}\rho}{\delta} \gg 1, \tag{23}$$

then equations 19 and 20 can be approximated by

$$\alpha_D \approx \alpha_I \approx -\frac{1+i}{2\omega}\cdot\frac{\rho}{\delta}. \tag{24}$$

Therefore, the ratio between α_D or α_I and α_L is given readily as

$$\frac{\alpha_D}{\alpha_L} \approx \frac{\alpha_I}{\alpha_L} = \frac{\rho}{z+h}, \tag{25}$$

which clearly shows that compared with the original electric field, the derivatives of D and I parts are enhanced as they depend mainly upon ρ, while the airwave, which is proportional to the water depth, increasingly is suppressed as the water becomes shallower. Therefore, taking derivative of the electrical field with respect to frequency can enhance the target signal, at the same time suppressing the effects of the airwaves. Interestingly, Maaø and Nguyen (2010) arrived at the similar conclusion by carrying out numerical simulations.

Approach 3: MT impedance stripping

At larger offsets, the lateral wave component of the measured horizontal electric field $\left(E_x^L\right)$ can be approximated as

$$E_x^L \approx \frac{p}{2\pi\sigma\rho^3}e^{-k(z+h)}, \tag{26}$$

which resembles a vertically propagating/diffusing plane wave. Note this is the same phenomena used to generate the source fields for the controlled source audio-magnetotellurics (CSAMT) method (Zonge and Hughes, 1991). Under this assumption, the horizontal electric and magnetic fields in a 1D earth satisfy

$$E_x^L = Z_{xy} \cdot H_y^L, \tag{27}$$

where H_y^L is the horizontal y-component of lateral-wave-generated magnetic field, and Z_{xy} is the plane wave or MT impedance of the medium. Because these fields are entirely horizontal, there is little sensitivity to the reservoir.

The impedance Z_{xy} can be obtained by making measurements of naturally occurring plane-wave fields via a marine MT survey. These data are measured during a MCSEM survey when the source is distant from the receivers such that the CSEM fields are smaller in amplitude than the naturally occurring fields, or when the source current is off. Using standard MT processing, the MT impedance is determined for a 1D earth as

$$Z_{xy}^{\mathrm{MT}}(f) = \frac{E_x^{\mathrm{MT}}(f)}{H_y^{\mathrm{MT}}(f)}, \tag{28}$$

where the $Z_{xy}^{\mathrm{MT}}(f)$ designates an estimate of the MT impedance made at the specific frequency used in the MCSEM survey. By multiplying the magnetic field measured in the MCSEM survey by the MT determined impedance, we can estimate the corresponding electric field that satisfies the plane-wave assumption, i.e., we can estimate the horizontal electric field that is generated by the lateral wave via

$$E_x^L \approx Z_{xy}^{\mathrm{MT}} \cdot H_y^{\mathrm{CSEM}}. \tag{29}$$

In theory, this approximation holds only when the offset between transmitter and receiver is large enough. However, in shallow water this is not so difficult to satisfy as it appears to be. Note that in shallow water H_y^{CSEM} generally varies very

Downloaded 11 Jun 2012 to 146.23.4.26. Redistribution subject to SEG license or copyright; see Terms of Use at http://segdl.org/

slowly, and is not as sensitive to a resistive target as is E_x^{CSEM}. As long as the offset is roughly five times the skin depth, for example 3 km in the shallow water case shown in Figure 1, we believe this approximation is valid. Subtracting this lateral-wave term from the measured electric field in the MCSEM will define a new quantity, which is called the "scattered" electric field $\left(E_x^{\mathrm{scat}}\right)$

$$E_x^{\mathrm{scat}} = E_x^{\mathrm{CSEM}} - Z_{xy}^{\mathrm{MT}} \cdot H_y^{\mathrm{CSEM}}. \tag{30}$$

Note that $Z_{xy}^{\mathrm{MT}} \cdot H_y^{\mathrm{CSEM}}$ essentially estimates the plane-wave component of the electric field which is insensitive to the reservoir. In practice for shallow water applications, usually we can find an overlapping frequency range where CSEM and MT data are recordable.

It should be noted that in 2D and 3D environments, the MT measured impedance is a 2×2 tensor rather than scaler. In general, the 3D tensor has the form:

$$\mathrm{Z}^{\mathrm{MT}} = \begin{pmatrix} Z_{xx} & Z_{xy} \\ Z_{yx} & Z_{yy} \end{pmatrix}. \tag{31}$$

In these cases, the MT impedance used in the expressions above would be the appropriate off-diagonal component after the impedance tensor has been rotated such that its components align with the MCSEM data. Finally, if no MT data were available at each site, but a numerical model existed that was constructed from other data, the estimated MT impedance could be calculated via a modeling step.

SYNTHETIC SHALLOW WATER MODEL STUDY

Detectability

To define detectability for a system, we compute the ratio of inline E_x fields between a reservoir model and a corresponding baseline model, i.e.,

$$detectability = \frac{E_x(target)}{E_x(baseline)} \approx 1 + \frac{\Delta E_x}{E_x(baseline)}, \tag{32}$$

where ΔE_x is the difference between the target and baseline model responses or the secondary response. Generally the detectability is a complex value, meaning that its amplitude and phase can be used. In this paper, however, we use the amplitude otherwise specified. The larger the detectability, the better the chance to detect the reservoir target. In this synthetic example we use a threshold value of 1.2 as a cutoff in presenting the synthetic responses.

Having defined the detectability, we think it is worthwhile illuminating more on detectability. What we define as detectability often is referred to as "normalized amplitude" or more loosely "sensitivity." The reason for us to distinguish detectability and sensitivity is that sensitivity is more appropriately used for inverse problems in which it represents the ratio of a data change to a model change.

As shown in equation 32, the model change is not explicitly taken into account in detectability; the value of detectability only shows how the data have been changed between the target and baseline models, no matter how large or small the model change is.

On the other hand, if we look at the expanded form of the inline $E_x(target)$ field, as shown in equation 32, we can see that detectability is related directly to the ratio of the secondary field ΔE_x over the baseline field.

This ratio is more or less an indicator of the chance that the target could be detected with a current acquisition system. In this sense, we think that detectability is a better term than normalized amplitude. Moreover, a noise threshold for the $E_x(baseline)$ field, say 1.0×10^{-15} V/(Am^2), should be added into the denominator in computing the detectability. This is important, especially in deep water where the inline E_x field usually is much less than its counterpart in shallow water; otherwise, a huge but false value of detectability is derived.

Deep water versus shallow water

To provide an understanding of the effects of the airwave, as well as to test the three mitigation methods, we have designed four 2D target scenarios as shown in Figure 4: a deepwater (water depth 3 km) model with a flat seafloor (DF), a shallow water model (water depth 0.1 km) with a flat seafloor (SF), a deepwater model with bathymetry (DB), and a shallow water model with bathymetry (SB). In all four scenarios, receivers are assumed to be deployed at the seafloor, and transmitters are kept 50 m above the seafloor. The reservoir target is a resistive slab (20 Ωm) with a length of 9 km, and a thickness of 50 m, about 1.6 km below the seafloor, and embedded in a four-layer seabed. Although the depth of the slab is different relative to the sea surface in deep and shallow water, its relative location below the seafloor remains the same. The variation of the bathymetry is roughly 1 km over a 30-km long profile. The corresponding background model without the slab target is used as the baseline model for calculating the detectability in each scenario.

In the computation of 2.5D MCSEM model responses, 68 inline electric dipoles, separated by 0.5 km, and 31 receivers with a spacing of 1 km, were used with the 2.5D forward algorithm described in Abubakar et al. (2008). Both inline E_x and crossline H_y components were simulated for the baseline and target models.

We tested the methods for a variety of frequencies ranging from 0.0625 Hz to 1.25 Hz. Here only 0.25 Hz data are presented because of space limitations. For the MT stripping approach, 2D MT impedance (TM mode) data were computed using a finite-difference algorithm, similar to the 3D FD code outlined in Newman and Alumbaugh (1995). The detectability is calculated as the ratio between the response with the target and the baseline model, and plotted and contoured as a function of transmitter and receiver position. Note that a noise floor of 1.0×10^{-15} V/(Am^2) for the electric field was assumed, and any computed field less than this floor was set to this value. By doing this, the computed ratio will guarantee that any anomaly, especially at larger offsets, that falls below standard noise levels will be excluded.

As shown in Figure 5, in deep water (models DF and DB in Figure 4a and c), with and without bathymetry, we have as much as a factor of 2 difference in signal between the target and background models, i.e., we have a maximum of 100% increase in the target response, compared to the background. On the contrary, in shallow water (models SF and SB in Figure 4b and d), the detectabilities are significantly smaller, suggesting that the reservoir is difficult to detect in these scenarios.

Downloaded 11 Jun 2012 to 146.23.4.26. Redistribution subject to SEG license or copyright; see Terms of Use at http://segdl.org/

Airwave-mitigated shallow water data

When we apply the three airwave-mitigating approaches to the shallow water data (with and without bathymetry), the detectability increases significantly. As shown in Figure 6, all three approaches provide for a reservoir response that stands out almost as well as if the data were acquired in deep water. This is especially true for the MT stripping approach, which seems to best reproduce the deepwater response. However, because we are combining the data in different ways to remove the airwave

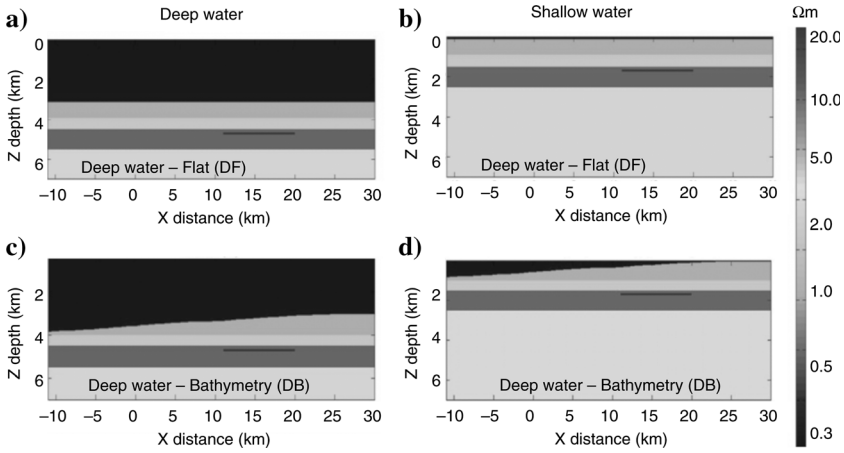

Figure 4. Four target resistivity (in Ω.m) models for testing the airwave-mitigation approaches. Figure 4a and c are two deepwater models with a flat (DF) and a bathymetric seafloor (DB). Figure 4b and d are their counterparts in shallow water (SF and SB). The four baseline models are the corresponding models without the thin slab reservoir target.

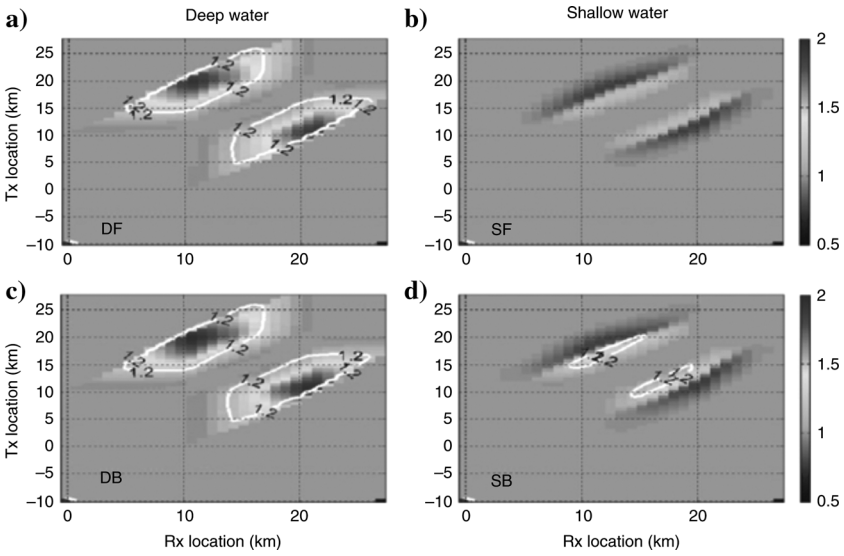

Figure 5. Detectabilities of the raw inline Ex fields to the slab target in the four scenarios shown in Figure 4. The horizontal axes represent Rx locations and the vertical Tx locations, i.e., each data point is associated with a specific pair of Tx and Rx location. Figure 5a and c are the detectabilities in deep waters, and Figure 5b and d are in shallow waters. The applied frequency was 0.25 Hz.

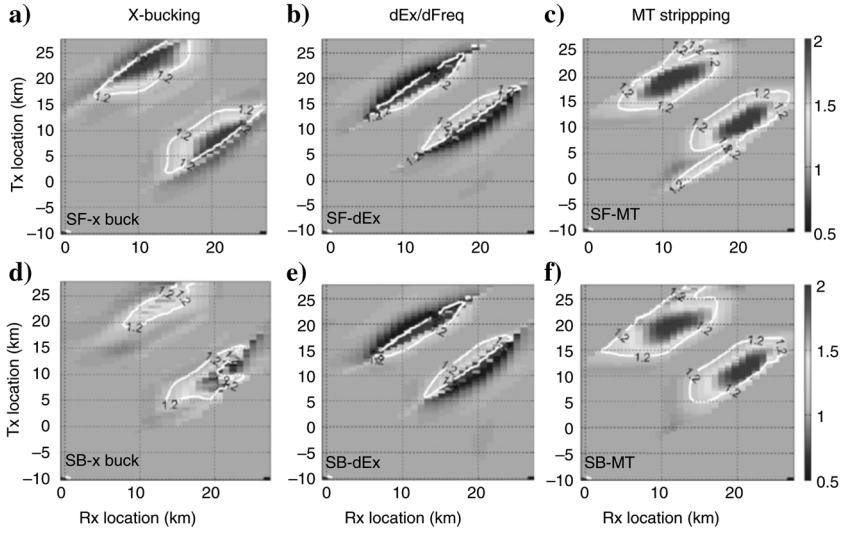

Figure 6. Detectabilities of the airwave-mitigated E_x fields for the two shallow water models (model SF on the top and SB on the bottom). The x-bucking is in 6a and d; dEx/dFreq is in 6b and e and MT stripping is in 6c and f. The applied frequency was 0.25 Hz.

Downloaded 11 Jun 2012 to 146.23.4.26. Redistribution subject to SEG license or copyright; see Terms of Use at http://segdl.org/

component, the various approaches exhibit different features. For example, using a bucking distance of 2 km, the lateral-bucking results resemble the MT stripping in the flat model because both approaches are designed to remove completely the airwave from the measured data.

On the other hand, the dEx/dFreq is aimed to reduce the airwave part relative to the other components. The dEx/dFreq data have relatively larger anomalies but are more focused in space and are accompanied by side lobes where the detectability is less than 1. Further discrepancies appear in the bathymetric models (Figure 6d–f). The lateral-bucking result shows characteristics that suggest that the bathymetry, coupled with the geometric errors in Tx locations, affects this method more than in the other two approaches. As a whole, these results demonstrate the possibility of these types of airwave mitigation approaches on MCSEM data collected in shallow water to enhance subsurface target responses.

During the synthetic study, what we found interesting was that at 0.0625 Hz or lower frequency the shallow water data are much less affected by the airwaves in a typical working Tx-Rx offset range, say, from 1 to 10 km. This can be explained by the fact that both the direct and image fields attenuate much more slowly than those at higher frequencies, resulting in the airwaves showing up at larger offsets. Because of this it seems that we can obtain enough signal to distinguish the reservoir target from its baseline background in shallow water at these lower frequencies.

In the above shallow water example, the detectability at 0.0625 Hz was about 30%. This suggests to us that in real surveys we could obtain information on the potential target of interest in shallow water by using 0.0625 Hz or lower frequency data without worrying about the effect of the airwaves. However, as shown by Alumbaugh et al. (2010), the resolution to the thin-resistor for lower-frequency guided mode is substantially decreased compared with higher-frequency modes.

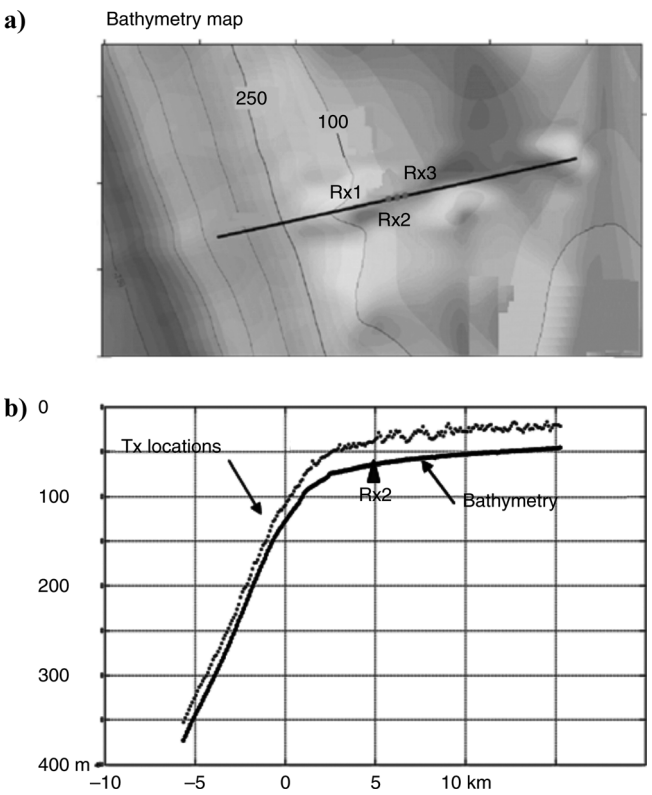

Figure 7. On the top is the bathymetry map of the shallow water MCSEM survey that was made along a single tow-line (the tow direction was eastward) of 21 km, and three receivers were deployed. On the bottom is the bathymetry and transmitter trajectory along the towline (the horizontal and vertical scales are not the same). Note that relatively larger uncertainties exist in the depth of transmitter in the shallower part. The water depth varies from 350 m in the west to 50 m in the east.

APPLICATION TO A REAL MCSEM SURVEY

Shallow water survey

To apply the three approaches to a real shallow water MCSEM data set, we make use of research data collected in an offshore area that cannot be identified here. In this small survey, a single 21 km-long towline was towed from west to east, as shown in Figure 7, where the bathymetry map shows that the water depth ranges from 350 m on the left to 50 m on the right. Three multiple component receivers (for electric and magnetic fields) were deployed in the central region with a spacing of 500 m. Conventional MCSEM data and marine MT data were acquired and processed. However, because of the time limitations in the data collection, we found that the amount of data available was not enough to provide adequate stacking for good quality of MT impedance data, which is required in the MT stripping method. Alternatively, for that purpose we used the computed 1D MT impedance generated from a recovered 1D resistivity model, which we believe is a good approximation to the real earth model.

Part of the experiment was to compare time- and frequency-domain MCSEM data. This allows us to explore both data sets separately, with a general understanding that in a short or middle range offset the airwave effect is recognizable easily and might be separated from measured TD data. Also as mentioned in the previous section, the FD 0.0625 Hz data show little effect of the airwave. Therefore, we can take advantage of these features to build a resistivity model, which would be biased if we could not handle the airwave effect well.

Considering that there are only three closely spaced receivers along a 21-km profile, a full 2D/3D analysis would be significantly time consuming and underdetermined. Therefore we focus on a 1D investigation for seeing how well we can mitigate the airwave effect. We chose the receiver in the middle, and used the outbound (in east) data to reduce the bathymetric effect. In Figure 7b, we can see that the sea bottom is roughly flat with a water depth of about 50 m, making the 1D analysis less problematic. At the same time, we recognize that the depth of the transmitter varies significantly, especially in shallow water. That will create a certain amount of uncertainty on the depth of the transmitter, which will impact the performance of the x-bucking approach, which explicitly requires this information.

One-dimensional resistivity model

We inverted the TD data (0.01 to 2 s) at offsets of 2 km and 4 km to recover a 1D resistivity model (see Figure 8), which we believe is a good representation of the resistivity structure along

Downloaded 11 Jun 2012 to 146.23.4.26. Redistribution subject to SEG license or copyright; see Terms of Use at http://segdl.org/

this line. This model was verified with 0.0625 Hz data, showing a satisfactory data fitting over offsets of 2 km to 10 km. As can be seen from Figure 8, this model reveals three resistors: the top one near the seabed, 3 Ω.m, the second one at about 700 m, with 7 Ω.m, and the third one, the resistive basement, about 30 Ω.m.

To evaluate our three methods, we determined how applying the three airwave-mitigation approaches changed the detectability to the bottom resistor, which is thought to be masked by the shallow resistors, as well as the airwaves.

Therefore, we treat the recovered model as the target model, and then the model with a constant basement resistivity (1.3 Ω.m) as a baseline model. We then can provide the detectability analysis as we did in the synthetic study.

Detectability analyses

For the original inline E_x data, the detectability was computed using equation 32 in which E_x (baseline) was the computed response generated from the baseline model shown in Figure 8. The corresponding detectability curves at four frequencies (0.1875 Hz to 0.5625 Hz) are shown in Figure 9a. Over the offset range of 1 to 10 km, we can see that the detectability is either close to or less than 1.0, suggesting we could not distinguish the target model from the baseline model with these original four frequencies' data. This is not a surprise, because the airwave and the shallow resistors are expected to mask the signal from the basement.

The x-bucking method was tested with three bucking distances, specifically 1 km, 2 km, and 4 km. Considering the data noise at different offsets and geometric errors (horizontal distance and vertical depth) for the Tx locations, we chose a bucking distance of 2 km.

The detectabilities for the 2 km are shown in Figure 9b. Again four frequencies were used. The results are rather noisy, and do not seem to support the presence of the resistive basement. At less than 5 km offsets, the values are almost 1; beyond that, the curves go up and down.

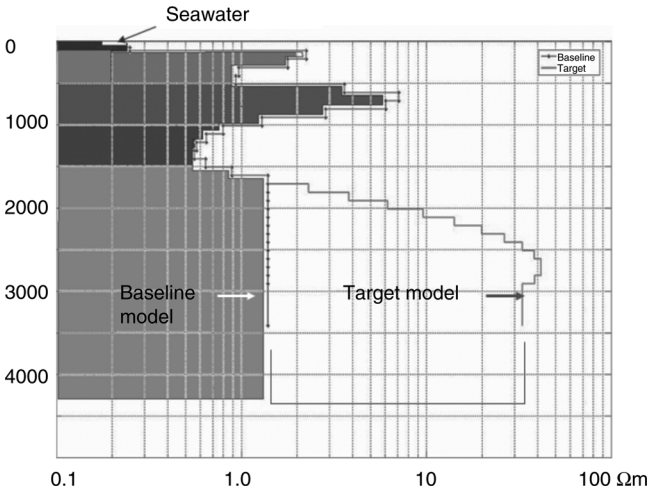

Figure 8. A recovered 1D resistivity model by inverting the TD data acquired at Rx2 in the shallow water survey. This model reveals three resistors near the mudline, in the middle, and in the basement. To do detectability analysis on the resistive basement, the basement is replaced with a constant resistivity of 1.3 Ω.m, and then this 1D model is regarded as the baseline model.

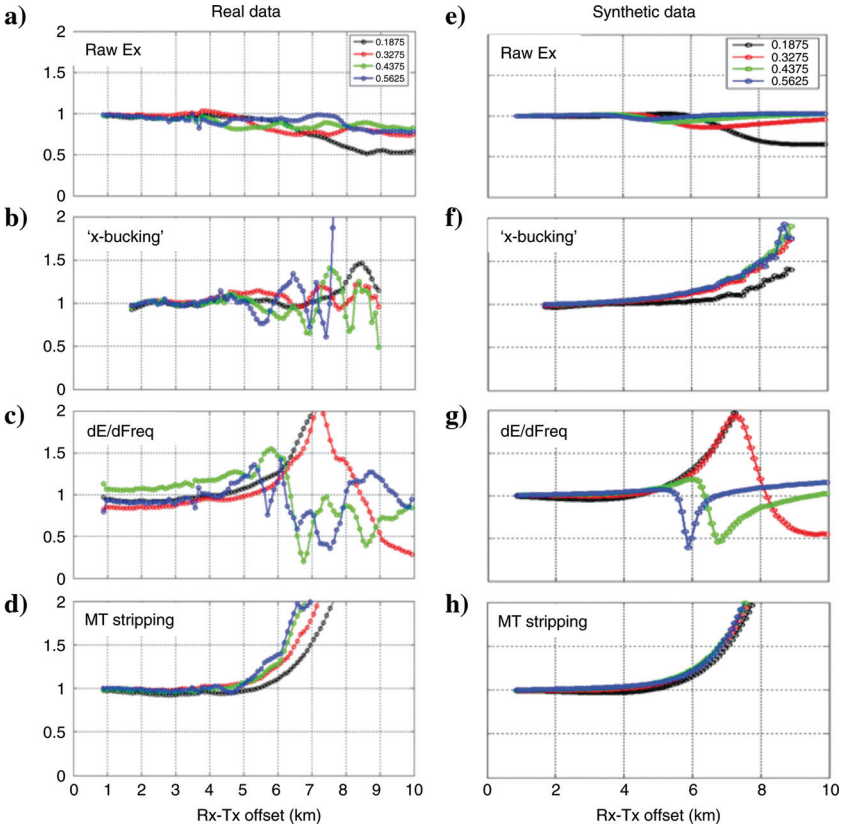

Figure 9. Comparisons of detectabilities of the original inline E_x, and airwave-mitigated data by the x-bucking, dE/dFreq, and MT impedance stripping methods. Four frequencies (0.1875, 0.3275, 0.4375, and 0.5625 Hz) were used. Figure 9e–h are the synthetic detectabilities for their counterparts.

Downloaded 11 Jun 2012 to 146.23.4.26. Redistribution subject to SEG license or copyright; see Terms of Use at http://segdl.org/

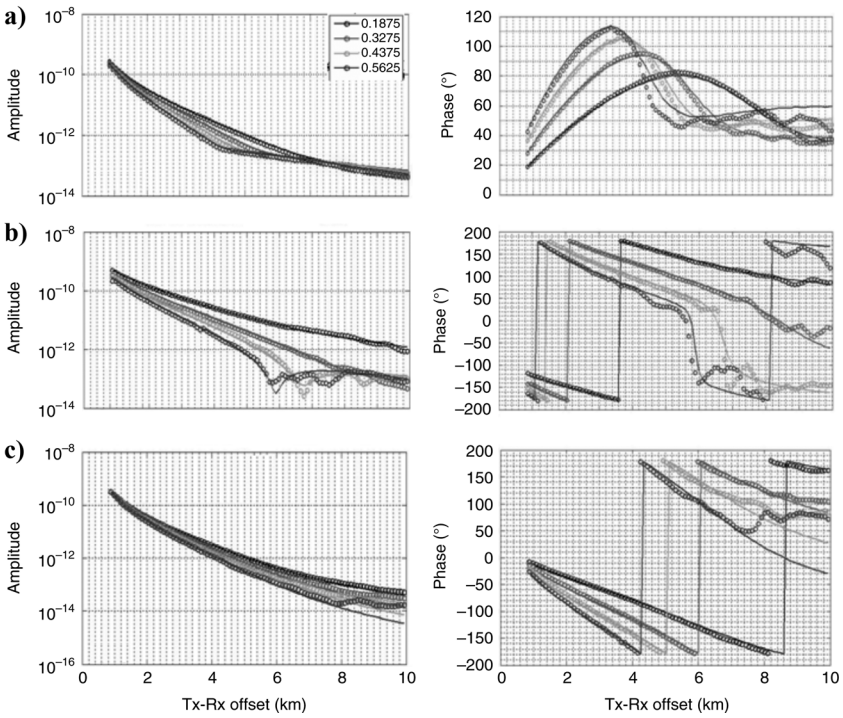

Figure 10. Comparisons of the observed and calculated inline E_x, dEx/dFreq, and MT impedance stripped data. (a) For the raw E_x data, (b) dEx/dFreq, and (c) MT stripped data. The calculated data were modeled from the recovered TD 1D resistivity model shown in Figure 8. Amplitude and phase data at four frequencies are in a reasonable agreement over an offset range of 1 to 10 km, although they do show more discrepancy at far offsets because of the data noise.

We suspect that this can be attributed to three factors. First as mentioned when discussing equation 13, the uncertainty on the location of the transmitter affects the performance of this method. A simplified uncertainty analysis on the depth difference shows that an error of 1 m uncertainty in the depth will cause 0.3% in the bucked data. This is a more serious issue compared with the other two methods, because we had to use two Tx locations in the bucking process.

Second, the bathymetry might be an issue, as seen in the 2D synthetic example. Third, the bucking process might amplify noise at long offsets where signal is smaller relative to short offsets. All these complications might make the dual-half-space approximation, which was used in the x-bucking breakdown in this case.

For the dE/dFreq method (see Figure 9c), the first two frequencies work well. The detectability at 0.1875 Hz increases and reaches to the limit value (2) of the plot at about 7 km. The 0.3125 Hz also shows a good enhancement. The two higher frequencies probably are affected by data noise, as well as by lack of sensitivity to the target. We realize that subtraction of data at two adjacent frequencies definitely will amplify the data noise, especially at longer offsets where data noise tends to be higher. This requires us to be aware of data quality when applying this method.

The MT stripping method works best in this case, as displayed in Figure 9d. As mentioned earlier, the measured MT data were not satisfactory for our purpose; instead we used the computed MT impedance from the target model. All four frequencies show that the detectabilities have been significantly enhanced, suggesting we could detect the resistive basement from its baseline model if we used the airwave-corrected data.

For comparison, we plotted the corresponding detectabilities (see Figure 9e–h) of the synthetic E_x, x-bucking, dEx/dFreq, and MT stripped data. The synthetic data were generated from the target and baseline models shown in Figure 8. Generally the synthetic detectabilities are comparable to those in the real data, except that the x-bucking method in the synthetic data shows a certain amount of detectability, while it is almost overwhelmed by the Tx location uncertainty plus data noise in the real measurements. The Tx depth variation is reflected clearly even in the synthetic detectability for the x-bucking, but almost is not visible for the other two methods.

To provide a complete view on the observed and airwave-mitigated data, we compare the original observed and calculated data generated from the 1D resistivity models shown in Figure 8. Because x-bucking does not help us much in this case, we drop it from plotting. As shown in Figure 10, they do show a satisfactory agreement in the amplitude and phase data. Note that for the observed E_x, a five-point smoothing was applied, and then dEx/dFreq and MT stripped data were calculated to suppress the noise.

CONCLUSIONS

We present a detectability analysis where three airwave-mitigation approaches are applied to synthetic MCSEM data generated from shallow water models that include 2D bathymetry. When analyzed without processing, the shallow water data show much less detectability than the corresponding deepwater data. However, with the help of the three airwave-correction methods, we gain back at least some of the detectability that is lost because of the airwave masking effect.

To a certain degree, the mitigated data appear to be equivalent to the data acquired in deep water. In addition, these three approaches can be applied to data acquired by standard MCSEM technology without change to acquisition methods or layouts. The application of these three methods to the real shallow water data has been demonstrated by the detectability analysis for the

Downloaded 11 Jun 2012 to 146.23.4.26. Redistribution subject to SEG license or copyright; see Terms of Use at http://segdl.org/

resistive basement in a simplified 1D situation. More analyses based upon complicated 3D scenarios might improve the reliability of the proposed methods.

Further research on how to evaluate the usefulness of airwave-mitigating methods in inverting of shallow water MCSEM data is needed to fully tackle this airwave masking problem. An interesting argument in the EM community is that the airwave effect could be taken care of by carrying out directly 1D or 2D or 3D inversions of measured raw MCSEM data, without removing or reducing the airwave from measurements. As far as we know, there is no conclusive consensus. Our reasoning is that unless the scattered field, which is the difference between the target model and the baseline model, is much greater than the data noise, direct inversions will not be able to recover the target of interest well. Take the shallow water case in Figure 1 as an example; one would not expect that the reservoir layer could be well resolved by inverting the data shown in Figure 1d, because the response difference between the target and the baseline model could fall off into data noise.

In terms of data misfit, which is the criteria to terminate an inversion job, the target and the baseline or a similar model could fit the data probably equally well. In other words, because of the airwave, there is lack of sensitivity or resolution to the hydrocarbon layer in this case. If we apply the airwave-mitigating approaches, however, a better recovery might be achieved. This might evolve into a better understanding of detectability, sensitivity, and appraisal of inversion result. We leave that to future work.

ACKNOWLEDGMENTS

We are grateful for all the help from management and colleagues at WesternGeco EM and EMI. We would like to thank especially Graeme Cairns and Christopher Nalepa for providing us the acquired MCSEM shallow water data, as well as the 1D resistivity model inferred from the TD data. We are indebted to the associate editor and three anonymous reviewers for their critical and helpful comments, which have prompted us to improve this paper.

REFERENCES

Abubakar, A., T. M. Habashy, V. L. Druskin, L. Knizhnerman, and D. Alumbaugh, 2008, 2.5D forward and inverse modeling for interpreting low-frequency electromagnetic measurements: Geophysics, **73**, no. 4, F165–F177, doi:10.1190/1.2937466.

Alumbaugh, D. L., N. H. Cuevas, J. Chen, G. Gao, and J. Brady, 2010, Comparison of sensitivity and resolution with two marine CSEM exploration methods: 80th Annual International Meeting, SEG, Expanded Abstracts, 3893–3897.

Amundsen, L., 2008, System and method for electromagnetic wavefield resolution: Patent Cooperation Treaty publication WO/2003/100467.

Andréis, D., and L. MacGregor, 2008, Controlled-source electromagnetic sounding in shallow water: Principles and applications: Geophysics, **73**, no. 1, F21–F32, doi:10.1190/1.2815721.

Bannister, P., 1984, New simplified formulas for ELF subsurface-to-subsurface propagation: IEEE Journal of Oceanic Engineering, **9**, 154–163, doi:10.1109/JOE.1984.1145620.

Chave, A. D., and C. S. Cox, 1982, Controlled electromagnetic sources for measuring electrical conductivity beneath the oceans 1. Forward problem and model study: Journal of Geophysical Research, **87**, 5327–5338, doi:10.1029/JB087iB07p05327.

Clough, J. W., 1976, Electromagnetic lateral waves observed by earth-sounding radars: Geophysics, **41**, 1126–1132.

Constable, S. C., 2003, Method and system for seafloor geological survey using vertical electric field measurement: Patent Cooperation Treaty publication WO2003104844.

Eidesmo, T., S. Ellingsrud, L. M. MacGregor, S. Constable, M. C. Sinha, S. Johansen, F. N. Kong, and H. Westerdahl, 2002, Sea bed logging (SBL), a new method for remote and direct identification of hydrocarbon filled layers in deepwater areas: First Break, **20**, 144–152.

King, R. W. P., M. Owens, and T. T. Wu, 1992, Lateral electromagnetic waves: Theory and applications to communications, geophysical exploration, and remote sensing: Springer-Verlag.

Løseth, L. O., and L. Amundsen, 2007, Removal of air-response by weighting inline and broadside CSEM/SBL data: 77th Annual International Meeting, SEG, Expanded Abstracts, 529–533.

Løseth, L. O., H. M. Pedersen, T. Schaug-Pettersen, S. Ellingsrud, and T. Eidesmo, 2008, A scaled experiment for the verification of the seabed logging method: Journal of Applied Geophysics, **64**, 47–55, doi:10.1016/j.jappgeo.2007.12.002.

Lu, X., L. J. Srnka, and J. J. Carazzone, 2005, Method for removing air wave effect from offshore frequency domain controlled-source electromagnetic sounding data: Technical report, Patent Cooperation Treaty publication WO2005010560.

Maaø, F. A., and A. K. Nguyen, 2010, Enhanced subsurface response for marine CSEM surveying: Geophysics, **75**, no. 3, A7–A10, doi:10.1190/1.3377054.

MacGregor, L., M. Tompkins, and D. Andreis, 2005, Electromagnetic surveying for hydrocarbon reservoirs: patent GB2411006.

Newman, G. A., and D. L. Alumbaugh, 1995, Frequency-domain modeling of airborne electromagnetic responses using staggered finite differences: Geophysical Prospecting, **43**, 1021–1042, doi:10.1111/j.1365-2478.1995.tb00294.x.

Nordskag, J. I., and L. Amundsen, 2007, Asymptotic airwave modeling for marine controlled-source electromagnetic surveying: Geophysics, **72**, no. 6, F249–F255, doi:10.1190/1.2786025.

Srnka, L. J., J. J. Carazzone, M. S. Ephron, and E. A. Eriksen, 2006, Remote reservoir resistivity mapping: The Leading Edge, **25**, 972–975, doi:10.1190/1.2335169.

van den Berg, P. M., A. Abubakar, and T. Habashy, 2008, Removing sea surface-related electromagnetic fields in performing an electromagnetic survey: Patent Cooperation Treaty publication WO/2008/054888.

Wait, J. R., 1961, The electromagnetic fields of a horizontal dipole antenna in the presence of a conducting half-space: Canadian Journal of Physics, **39**, 1017–1028.

Weidelt, P., 2007, Guided waves in marine CSEM: Geophysical Journal International, **171**, 153–176, doi:10.1111/j.1365-246X.2007.03527.x.

Weiss, C. J., 2007, The fallacy of the shallow-water problem in marine CSEM exploration: Geophysics, **72**, no. 6, A93–A97, doi:10.1190/1.2786868.

Young, P., and C. S. Cox, 1981, Electromagnetic active source sounding near the east Pacific rise: Geophysical Research Letters, **8**, 1043–1046, doi:10.1029/GL008i010p01043.

Ziolkowski, A., and D. Wright, 2007, Removal of the airwave in shallow-marine transient EM data: 77th Annual International Meeting, SEG, Expanded Abstracts, 534–538.

Zonge, K. L., and L. J. Hughes, 1991, Controlled source audio-frequency magnetotellurics, *in* M.N. Nabighian, ed., Electromagnetic methods in applied geophysics, vol. 2, 713–809: SEG.

Downloaded 11 Jun 2012 to 146.23.4.26. Redistribution subject to SEG license or copyright; see Terms of Use at http://segdl.org/